Evidence for surface fusion in inertial electrostatic confinement devices

Richard Bowden-Reid,[1,a)] Joe Khachan,[1,b)] Jan-Philipp Wulfkühler,[2,c)] and Martin Tajmar[2,d)]
[1]*Department of Plasma Physics, School of Physics, University of Sydney, Sydney 2006, Australia*
[2]*Institute of Aerospace Engineering, Technische Universität Dresden, 01062 Dresden, Germany*

(Received 23 August 2018; accepted 22 October 2018; published online 6 November 2018)

Inertial electrostatic confinement is a method of producing nuclear fusion in which concentric spherical electrodes are used to accelerate ions to fusion relevant energies. Fusion events are generally attributed to collisions between accelerated ions and neutral gas molecules in the centre of the device, with ion–grid collisions considered detrimental. In this paper, we present data that indicate that collisions between ions and neutral gas molecules adsorbed on the grid surface may, in fact, contribute significantly to the observed fusion rate in deuterium fuelled systems. When operating in the 1×10^{-4}–1×10^{-3} Torr, $V \leq 40$ kV regime, fusion on the grid surface is found to contribute up to 80% of the measured fusion rate, as determined from hysteresis effects between the fusion rate and system pressure. Surface fusion measurements were also carried out for a selection of cathode materials, with graphite found to produce a fusion rate that is an order of magnitude greater than the highest performing metal targets. *Published by AIP Publishing.*
https://doi.org/10.1063/1.5053616

I. INTRODUCTION

Inertial electrostatic confinement (IEC) is a method for producing nuclear fusion in small scale devices. Originally proposed by Lavrent'ev[1–3] and further developed by Farnsworth[4,5] and Hirsch,[6–8] the concept makes use of concentric, spherical electrodes to trap and heat ions to fusion relevant energies.

Early theoretical approaches by Farnsworth and Hirsch assumed perfectly spherical, highly ionised systems in which the electron motion and ion motion are determined exclusively by the electric potential. Ion-ion fusion rates were subsequently calculated as

$$\mathcal{F} \approx n_1 n_2 \langle \sigma v \rangle_{avg}, \tag{1}$$

where n_1 and n_2 are the densities of the fusing fuels and $\langle \sigma v \rangle_{avg}$ is the distribution averaged reactivity.

No such an IEC system has been built, however, with practical devices instead of operating in the low ionisation, low current discharge regime,[9–12] often with electron injection,[13,14] ion injection,[15–17] or RF initiation.[18–20]

Ion motion in the discharge regime is mediated by momentum transfer and charge exchange interactions with background gas molecules, and so, the observed ion energy distributions vary significantly from those obtained through simple examination of the electric potential. Previous work[9,18] has shown that at elevated pressures (1×10^{-3}–1×10^{-2} Torr), peak ion energies may be as little as one quarter of the applied grid voltage. Coupled with low ion densities (10^8–10^{10} cm^{-3}),[21] this has led to ion-ion interactions often being neglected as a significant source of fusion with attribution instead being placed on ion-neutral collisions. IEC devices are therefore most accurately described as beam-target systems, in which energetic particles are incident on low energy target atoms.

Fusion targets may exist as free molecules within the gas volume or be adsorbed on, or embedded within, the cathode surface. The relative magnitudes of gas verses surface fusion may be explored through examining the area density of targets traversed by an ion in the gaseous and surface domains. Hirsch[7] used statistical arguments to approximate the ratio of recirculating (I_r) and collected (I_c) ion currents within an IEC device as

$$\delta = \frac{I_r}{I_c} \approx \frac{\eta}{1-\eta^2}, \tag{2}$$

where η: $0 \rightarrow 1$ is the transparency of the cathode. Evaluating the expression for $\eta = 0.98$, a practical upper limit on grid transparency gives $\delta = 25$. It is therefore expected that an average ion within the device will complete no more than 25 transits of the core before being lost to the grid. The total target area density is subsequently estimated as

$$\mathcal{N}_{gas} \approx 2\delta R_c n_{gas} = 2\delta R_c P / k_B T, \tag{3}$$

where n_{gas} is the gas number density, P is the system pressure, R_c is the cathode radius, k_B is the Boltzmann constant, and T is the gas temperature. Table I gives indicative gas target densities for published IEC devices.

Adsorption and implantation of hydrogen and deuterium in metal surfaces have been well studied. Although surface hydrogen layers are very thin (0.1–100 nm), the corresponding target densities may be many orders of magnitude larger than those found within the background gas. The target area density is given by

$$\mathcal{N}_{surf} = n_{surf} d_{surf} \approx \mathcal{N}_{ads} + \int n_{emb}(x) dx, \tag{4}$$

where n_{surf} and d_{surf} are the density and thickness of the surface layer, respectively. These terms may be re-written

a)Electronic mail: richard.bowden-reid@sydney.edu.au
b)Electronic mail: joe.khachan@sydney.edu.au
c)Electronic mail: jan-philipp.wulfkuehler@tu-dresden.de
d)Electronic mail: martin.tajmar@tu-dresden.de

TABLE I. Calculated target area densities for indicative IEC systems. In all cases, the gas temperature has been assumed to be 300 K.

R_c (cm)	η	P (Torr)	$\mathcal{N}_{gas}$ (cm^{-2})
6.25[a]	0.85	2.5×10^{-2}	3.08×10^{16}
10[b]	0.95	2.5×10^{-3}	1.57×10^{16}
5[c]	0.92	4.0×10^{-3}	7.71×10^{15}
5.5[d]	0.85	7.5×10^{-4}	8.13×10^{14}

[a]Reference 10.
[b]Reference 13.
[c]Reference 14.
[d]Reference 16.

according to the surface density of an atomically thin adsorption layer, $\mathcal{N}_{ads}$, and the line integrated density of the embedded layer. Table II gives the literature values for measured hydrogen target densities in both the adsorbed and embedded regions of various metals.

It is important to note that the area density of fusion targets encountered at the surface of the cathode is, in all cases, comparable to the number of gas targets encountered during an ion's entire lifetime within the focusing region.[22–24] Furthermore, it is found that after bombardment with 25 keV D^+, at relatively modest fluences ($1–2 \times 10^{18}$ cm^{-2}), the embedded density within metal samples may exceed the number of gas targets by more than an order of magnitude.[25]

Although numerous computational and experimental studies relating to surface and gaseous fusion sources in IEC machines have been performed,[26–29] it is not immediately clear which fusion region will dominate in any given IEC device. Achievable fusion rates may depend strongly not only just on system operating parameters but also on the materials from which the device is constructed. The cathode material and temperature may prove to be dominant factors in determining the ultimate fusion output.

In Sec. III, an experiment is described by which the relative contributions due to gaseous and surface fusion are studied for a set of traditional IEC cathodes. Step function changes in system pressure are used to examine how the fusion rate evolves as a function of time. In Sec. IV, the dependence of the surface fusion rate on the cathode material is explored.

TABLE II. Indicative hydrogen target densities on selected metal surfaces.

Material	$\mathcal{N}_{ads}$ (cm^{-2})	$\sim n_{emb}$ (cm^{-3})	$\sim d_{emb}$ (nm)	$\mathcal{N}_{emb}$ (cm^{-2})
Ni[a]	3.4×10^{14}			
W[b]	1.4×10^{15}			
Mo[c]	1.26×10^{15}			
Ta[c]	$\sim 4.2 \times 10^{15}$			
Nb[c]	$\sim 4.2 \times 10^{15}$			
Cu[d]		8.6×10^{21}	200	2.9×10^{17}
Ti[d]		7.1×10^{21}	272	6.0×10^{17}
SS[e]		4.7×10^{21}	372	2.3×10^{17}

[a]Reference 22.
[b]Reference 23.
[c]Reference 24.
[d]Reference 25.
[e]Stainless Steel; Ref. 25.

II. EXPERIMENTAL APPARATUS

Experiments were conducted in a 300 × 300 mm cylindrical vacuum chamber as depicted in Fig. 1. Prior to all experiments, the chamber was evacuated to below 1×10^{-6} Torr. IEC cathodes were suspended from a 5 mm diameter copper support rod insulated with nested layers of alumina ceramic tubing. The total insulation thickness was ∼3 mm. The chamber served as the anode. A pair of 150 mm diameter stainless steel IEC grids of different styles were produced;[30] see Fig. 2. A disc grid was assembled from annuli laser cut from 1 mm thick sheet metal. The annuli were slotted such that the longitudinal rings keyed into a single equatorial ring before being spot welded at the poles. An additional pair of wire rings was added by threading a 1 mm stainless steel wire through holes drilled in the longitudinal rings. A buckyball style grid was manufactured using sintered metal 3D printing. The grid consisted of a spherical shell 2.5 mm thick, with thirty two 45 mm circular openings. Neither grid had previously been exposed to deuterium.

An electron gun was constructed in the lower port of the vacuum chamber using an array of 50 W tungsten filaments as a thermionic electron source. The filaments were heated by a variable 0–9 V, floating AC power supply and were biased negatively with respect to the chamber between 100 and 2000 V. A grounded molybdenum extraction mesh served to accelerate thermionic electrons and electrically isolate the electron gun port from the main chamber. Electron gun currents between 10 and 150 mA were used to modulate the IEC discharge current at low pressures.

Deuterium gas was obtained through reverse fuel cell electrolysis of Deuterium Oxide. D_2O (99.9%) was obtained from Sigma-Aldrich and electrolysed using a HydroFill Pro fuel cell module. The generated D_2 gas was stored as a metal deuteride in HydroStik canisters. D_2 was emitted to the chamber through a leak valve, providing high resolution

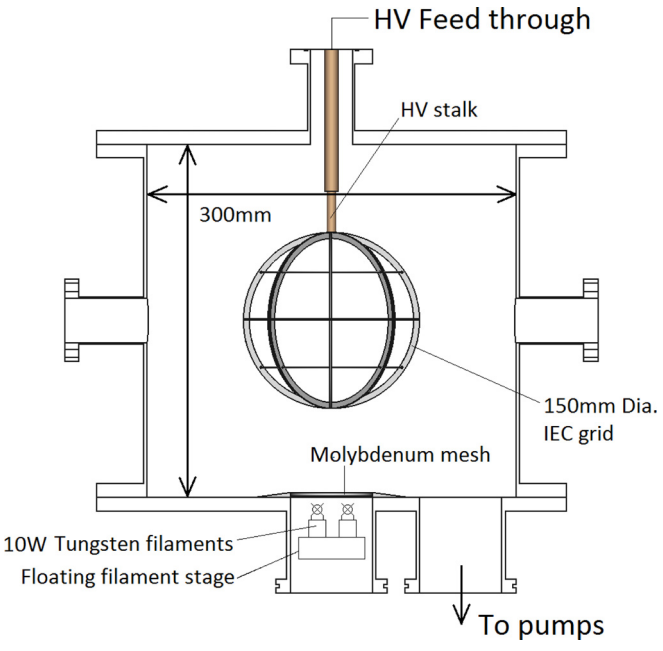

FIG. 1. IEC vacuum system.

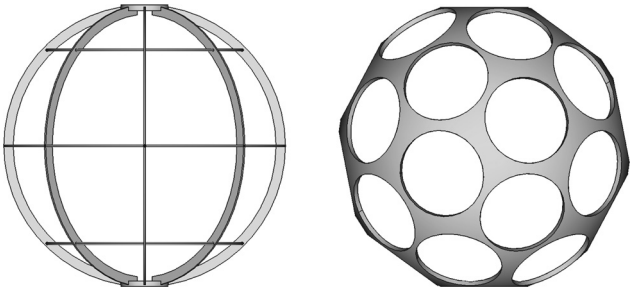

FIG. 2. IEC grids. Disk grid (left): area = 294 cm^2 and transparency = 92.6%. Buckyball grid (right): area = 358 cm^2 and transparency = 82.7%.

pressure control between 1×10^{-6} and 1×10^{-1} Torr. A Pfeiffer PKR251 compact pressure gauge was used to monitor the system pressure.

The D(d,n)^{3}He fusion reaction was monitored by fast neutron detection. Two 25 × 150 mm, 4 atm Helium-3 detectors with high density polyethylene moderator were placed 400 mm from the centre of the vacuum chamber and powered by a Canberra Scientific 3106D power supply. The detectors were operated at 1150 V. A model 3406D Picoscope was used to capture the output signal from the neutron detectors and was capable of recording a ten second snap shot every half minute. Each snapshot was recorded with a corresponding time stamp, along with the system voltage and discharge current.

The detectors were calibrated against a 12.5 cm Bonner Sphere detector which has a known response factor of 0.162 cm^2 for 2.45 MeV neutrons.[31]

III. PRESSURE HYSTERESIS IN IEC DEVICES

A. Experimental method

The buckyball grid was installed in the vacuum chamber, and the grid was conditioned in hydrogen at 40 kV 1 mA for several hours before being allowed to cool. A 35 kV, 500 μA hydrogen discharge was initiated at 1×10^{-2} Torr, and the system was allowed to run for a further 30 min to ensure that the grid temperature had stabilised. The hydrogen supply was swapped with deuterium, and the fusion rate was monitored until an equilibrium was reached at which time the pressure was lowered to 1×10^{-4} Torr. The discharge current was maintained at 500 μA through adjustment of the electron gun current. The decay in the fusion rate was monitored for a further 120 min. The current normalised fusion rate as a function of time is given in Fig. 3. It should be noted that while care was taken to maintain the discharge current at 500 μA, small fluctuations of ±10% were unavoidable. We present current normalised rates for this reason.

The disc grid was treated to an identical pre-conditioning as described above and was similarly exposed for changing the system pressure while maintaining a constant discharge of 35 kV and 350 μA. A hydrogen discharge was initiated at 1×10^{-4} Torr, and a 30 min pre-heat was conducted before deuterium was introduced and the fusion rate was monitored until an equilibrium was reached. Over the following 200 min, the pressure was increased in steps to 1×10^{-3}, 5×10^{-3}, and finally 1×10^{-2} Torr. Electron gun currents were predetermined in order to maintain a constant 350 μA discharge current over the pressure ranges. The period over which the pressure and electron gun values were adjusted generally lasted no more than 30 s. After a further 100 min of run time, the pressure was once again lowered to 1×10^{-4} Torr and the decay in the fusion rate was observed. The time varying fusion rate for the disc grid is given in Fig. 4, while the region averaged fusion rate as a function of pressure is given in Fig. 5. Optical spectroscopy of the H_α (656.28 nm) and D_α (656.10 nm) Balmer lines later confirmed that the hydrogen-deuterium transition period lasted no more than 3–5 min. These experiments constituted the first exposure of both grids to deuterium gas.

B. Results and discussion

For a system in which both gaseous fusion and surface fusion occur, we can approximate the total fusion rate as

$$\mathcal{F} \approx \frac{I_c \sigma}{e}\left[\mathcal{N}_{gas} + \mathcal{N}_{ads} + \mathcal{N}_{emb}\right], \tag{5}$$

where I_c/e is approximately the ion fluence rate, σ is the distribution averaged fusion cross section, and $\mathcal{N}$ is the area density of targets in a given region. For small variations in pressure, we expect $\mathcal{N}_{gas}$ and hence the corresponding fusion

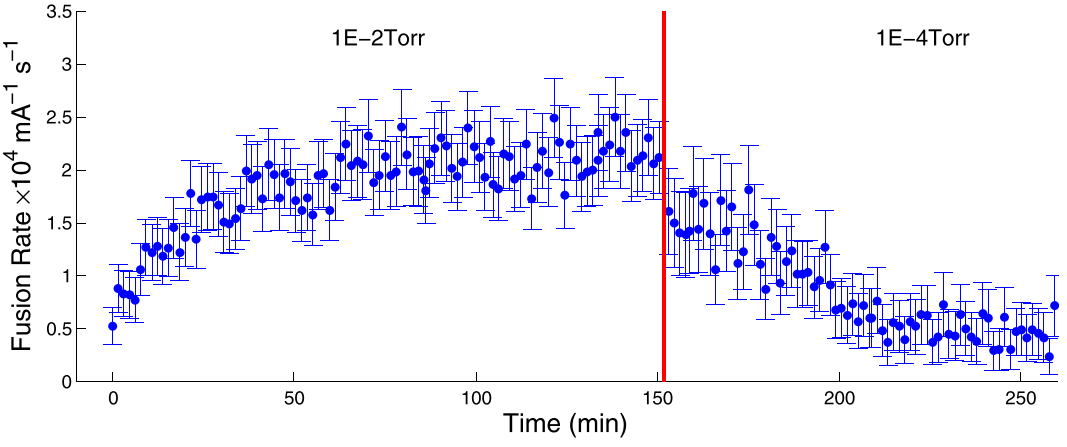

FIG. 3. Buckyball grid fusion rate as a function of time for changing the system pressure. 35 kV and 500 μA. The vertical line indicates the pressure change, and each region is labelled according to pressure.

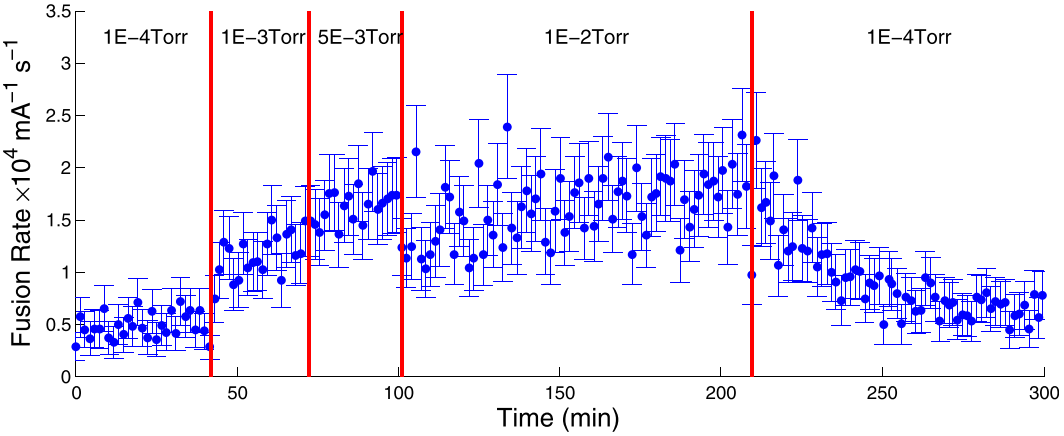

FIG. 4. Disc grid fusion rate as a function of time for changing the system pressure. 35 kV and 350 μA. Vertical lines denote pressure changes, and each region is labelled according to pressure.

contribution to scale proportionally. Larger changes in pressure are expected to deviate from linearity as the number of ion-neutral collisions moderate ion motion and hence alter the average cross section. $\mathcal{N}_{ads}$ depends on the balance of adsorption and desorption at the cathode surface given as

$$\frac{d\theta}{dt} \approx \nu_a(1-\theta)^2 \exp\left(\frac{-E_a}{k_B T_g}\right) - \nu_d \theta^2 \exp\left(\frac{-E_d}{k_B T_s}\right), \quad (6)$$

$$\theta = \mathcal{N}_{ads}/\mathcal{N}_0, \quad (7)$$

where $\mathcal{N}_0$ is the surface density of adsorption sites, θ is the occupancy fraction, and $\nu_{a,d}$ and $E_{a,d}$ are the frequency factors and activation energies for adsorption and desorption, respectively. $T_{g,s}$ are the temperatures of the gas above the surface and the surface, respectively.

In the case of constant temperature $T_g = T_s = T$, Eq. (6) can be solved to give $\theta(t)$ in the form of a hyperbolic tangent function

$$\theta(t) = \gamma_1 - \gamma_2 \tanh[\gamma_3(t - t_0)], \quad (8)$$

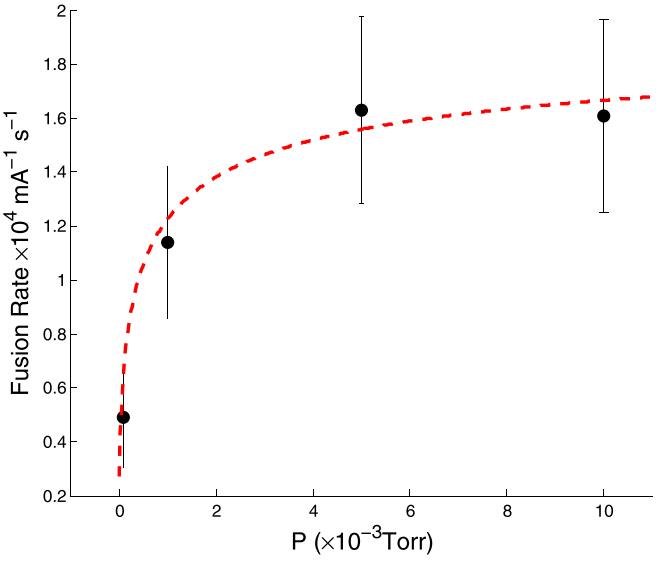

FIG. 5. Disk grid fusion averaged over regions of constant pressure. Fitted Langmuir isotherm for dissociative adsorption is given by the dashed line.

where γ_i are constants that depend on $\mathcal{N}_0$, $\nu_{a,d}$, and $E_{a,d}$. Setting Eq. (6) to zero and solving for the steady state gives the well-known result for the surface coverage as a function of pressure, known as the Langmuir isotherm for dissociative adsorption

$$\theta = \frac{\sqrt{K_{eq}P}}{1 + \sqrt{K_{eq}P}}, \quad (9)$$

where K_{eq} is an equilibrium constant. It has been assumed that the adsorption frequency coefficient, ν_a, is proportional to the neutral particle flux and hence the pressure. Finally, $\mathcal{N}_{emb}$ is given by a balance of the ion implantation rate and subsequent diffusion of ions back to the cathode surface where desorption may occur. We consider embedded fusion to be a minor contribution as will be discussed.

It is immediately apparent from Figs. 3 and 4 that the observed fusion rates are not consistent with a model in which gas fusion dominates. The fusion rate for the buckyball grid is seen to rise very slowly, taking in excess of an hour to stabilise. The initial fusion rate, corresponding to the gaseous fusion rate, contributes only 23% of the final total, indicating that 77% of the observed fusion occurs at the cathode surface. The asymptotic approach is the result of time dependent accumulation of surface deuterium, whether through gas adsorption or ion implantation. The extensive conditioning procedure rules out changes in the surface morphology as a contributing factor.

Note in Fig. 3 that when the system pressure, and hence $\mathcal{N}_{gas}$, was suddenly reduced by two orders of magnitude at 150 min, the fusion rate did not drop sharply as expected by a gas fusion model. Instead, the short term fusion rate remained relatively constant with only a small step reduction of ∼20% observed. It is possible that this gives a further measure of the gaseous contribution to the total; however, as a corresponding effect is not observed in the disc grid results, we regard the result as anomalous.

Following the initial step in Fig. 3, the fusion rate decays to match the new system conditions over a further ∼50 min. Such behaviour is consistent with the gradual desorption of gas from the cathode as described by Eq. (6). The reduction in pressure results in a corresponding drop in

the adsorption frequency factor, ν_a, leaving desorption as the dominant process. The surface coverage and hence fusion rate decay according to Eq. (8).

Note that the results for the disc grid in Fig. 4 display a distinct departure in behaviour from that observed in the buckyball system. The step function increases in operating pressure resulted in corresponding step function responses in the fusion rate. The exponential approach as measured previously is absent, and it is expected that this is the result of the initial pre-heat conditions chosen for the two grids. In the case of the buckyball grid, the system pre-heat in 10^{-2} Torr hydrogen would have saturated the cathode surface with non-fusible targets. When the inlet gas was exchanged with deuterium, the accumulation of fusion targets on the grid was limited by the hydrogen-deuterium exchange rate. By contrast, the disc grid was initially held at low pressure such that when additional deuterium was introduced to the system, fusible targets were rapidly deposited on vacant binding sites. This observation further accounts for the marked similarity in time constants when comparing the rise and fall times for the buckyball grid. If the exponential rise in the deuterium concentration is considered instead as an exponential decline of hydrogen coverage in response to a lowering of the partial pressure of hydrogen in the vacuum, we see that the two processes are equivalent and should be expected to exhibit a similar dynamic behaviour. The cool down period of several hours following the conditioning of the grids was evidently long enough to purge the grids of hydrogen adsorbed during this process.

The rising steps in Fig. 4 are partially consistent with gas fusion, that is, rapid increases in pressure result in immediate increases in the fusion rate. The 5×10^{-3} to 1×10^{-2} Torr transition at $t = 100$ min is of interest due to the initial reduction in the fusion rate followed by a gradual recovery. It is postulated that this is the effect of ion moderation by the background gas, initially reducing the fusion cross section, followed by a slow rise in the number of adsorbed deuterium targets due to improved convective cooling of the cathode.[14]

In order to differentiate gaseous and surface sources, the region averaged fusion rates were plotted against pressure and are given in Fig. 5. A Langmuir isotherm was fitted and found to be in excellent agreement with the observed fusion data. The fusion rate therefore appears to obey the form

$$\mathcal{F} \approx \frac{I_c \sigma}{e} \mathcal{N}_{ads} = \frac{I_c \sigma}{e} \cdot \frac{\mathcal{N}_0 \sqrt{K_{eq} P}}{1 + \sqrt{K_{eq} P}}, \tag{10}$$

which is consistent with a surface fusion model.

Finally, the embedded contribution to the fusion rate must be addressed. During the experiment, the disc grid experienced an ion flux of $\sim 3.7 \times 10^{12}\,\mathrm{cm}^{-2}\,\mathrm{s}^{-1}$, resulting in a total fluence of $4.5 \times 10^{16}\,\mathrm{cm}^{-2}$ over the first 200 min of operation. Given the data in Table II, it is expected that the area density of embedded deuterium would increase from zero to approximately $6.5 \times 10^{15}\,\mathrm{cm}^{-2}$ over this period. The absence of an obvious increasing trend in the fusion data, particularly over the 100–200 min interval, suggests that embedded fusion does not contribute significantly to the total.

IV. FUSION ON METAL SURFACES

It has been shown in Sec. III that the fusion rates measured in IEC systems display pressure and time dependencies consistent with surface fusion between energetic ions and adsorbed targets. The area density of targets on the metal surface, therefore, becomes an important consideration when designing new IEC systems. We wish to study the dependency of the surface fusion rate on the cathode material and so a 44 mm diameter stainless steel sample stage was constructed and fastened to the end of the high voltage stalk, in place of the IEC grid in Fig. 1. Rectangular samples (30×35 mm) of various materials were prepared in order to study the material dependence of the fusion rate in a deuterium discharge. The planar cathodes do not allow recirculation and hence eliminate almost all background gas fusion.

A. Experimental method

Samples of 316 Stainless Steel, Titanium, Molybdenum, Copper, Silver, and Graphite were prepared. The pieces were thoroughly cleaned with methanol and affixed to the sample stage. Following pump down, deuterium gas was introduced and the pressure raised to 1×10^{-3} Torr. The sample was allowed to soak for 15 min before a 35 kV, 1 mA discharge was initiated and the fusion rate monitored as a function of time. As the samples were not previously conditioned for high voltage operation, the first few data points tended to be anomalously high due to arcing. These points were discarded. Arcing generally subsided within 45–90 s.

Once the fusion rate had reached an equilibrium, the pressure was lowered to 5×10^{-4} Torr and finally to 1×10^{-4} Torr. Fusion measurements for each sample were conducted over about 15 min at each pressure.

B. Results and discussion

Fusion rates as a function of time for select cathode materials are given in Fig. 6. Rates have been normalised to their initial values such that the trends may be compared. Both titanium and copper exhibit behaviour comparable to that of molybdenum, and so, these samples have been excluded for clarity. Unlike the grids in Sec. III, the planar cathodes were not pre-heated in hydrogen, and hence, the fusion rate evolves as the cathodes heat in the discharge. At low pressures, radiative heat loss dominates, and so, we may express the power balance as

$$\mathcal{C} \frac{dT}{dt} = \left[\frac{1}{2} IV + A\sigma (T_0^4 - T^4) \right], \tag{11}$$

where T is the temperature of the sample, I and V are the system current and voltage, respectively, A is the cathode area, and σ is the Stephan-Boltzmann constant. A factor of one half is introduced to account for the approximate fraction of electrical power that is deposited into the cathode as opposed to the chamber wall. T_0 is the ambient temperature, and $\mathcal{C}$ is the thermal capacitance of the cathode, given by the product of its mass and the specific heat capacity of the material from which it is made. It is assumed that the thermal capacitance of the cathode is dominated by that of the sample

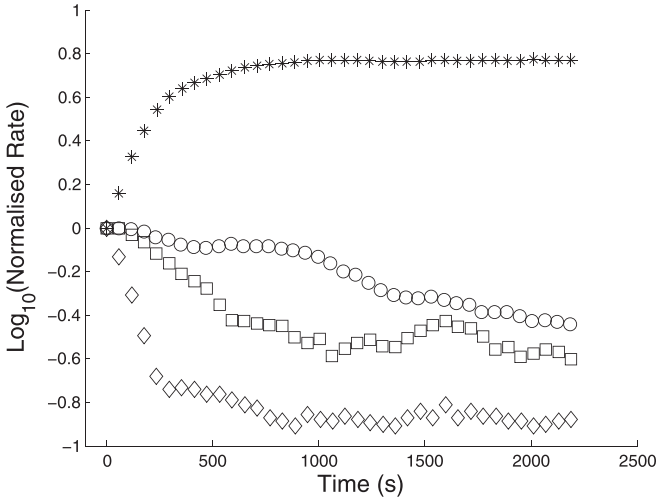

FIG. 6. Evolution of the fusion rate as a function of time for select cathode materials. ◇ = 316 stainless steel, □ = Molybdenum, ○ = Silver, and * = Graphite.

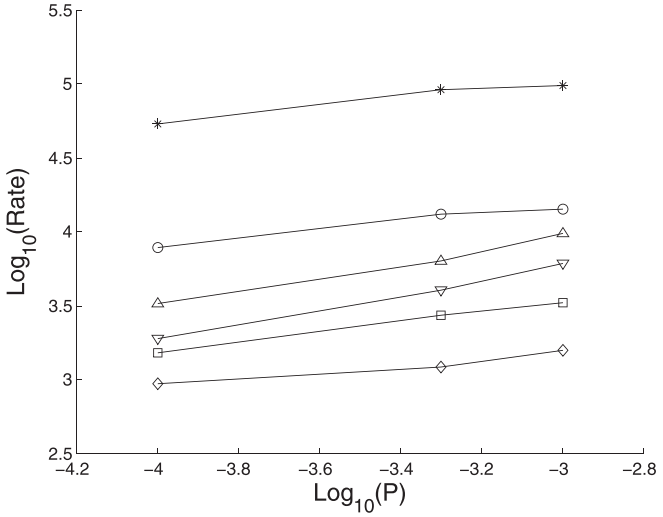

FIG. 7. Surface fusion rate as a function of pressure for various cathode materials. Values are normalised to the initial rate. ◇ = 316 stainless steel, □ = Molybdenum, ▽ = Copper, △ = Titanium, ○ = Silver, and * = Graphite.

holder, with additional contributions due to the material samples regarded as negligible. Equation (11) may be solved to give an implicit form for $T(t)$ as

$$t + t_0 = \frac{\mathcal{C}}{4\gamma_1^3\gamma_2}\left[\ln(\gamma_1 + \gamma_2 T) - \ln(\gamma_1 - \gamma_2 T)\ldots + 2\tan^{-1}(\gamma_3 T)\right], \tag{12}$$

where t_0 is the integration constant, and the following abbreviations have been used:

$$\gamma_1 = \left(\frac{1}{2}IV + \sigma A T_0^4\right)^{1/4},$$
$$\gamma_2 = (A\sigma)^{1/4},$$
$$\gamma_3 = \gamma_2/\gamma_1.$$

Equation (12) has been used to compute the heating profile, estimating an equilibrium temperature of ∼550 K, after ∼500 s.

All metal samples display a decaying trend in the fusion rate with increasing temperature, consistent with the thermal desorption of adsorbed deuterium from the cathode surfaces. This deleterious effect of cathode temperature on the fusion rate has also been observed in gridded IEC systems.[32] As the samples were exposed to approximately the same heating profiles, the varying decay rates for the different metals provide insight into the relative magnitudes of the activation energies $E_{a,d}$ in Eq. (6). In this way, the time series are reminiscent of thermal desorption spectroscopy (TDS) measurements in which samples are heated at a known rate in order to promote desorption and study gas trapping mechanisms.[33] While a detailed analysis of the material results will be left as future work, it is noted that materials with larger equilibrium fusion rates also exhibit longer time constants during the decay phase. Stainless steel, the poorest performing material tested, undergoes rapid loss of deuterium for only modest increase in temperature, while the silver sample does not reach equilibrium even after 1500 s at 550 K.

Contrasted against the metal samples, graphite displays unique behaviour. Graphite appears to accumulate additional surface targets over the first 500 s, leading to an almost 10-fold increase in the fusion rate. TDS measurements have shown that very high temperatures (>800 K) are required to liberate trapped hydrogen from graphite samples,[34] far higher than those obtained during this experiment. The second term in Eq. (6) is therefore set to zero, leading to monotonically increasing surface coverage. It is expected that IEC cathodes constructed from graphite would be capable of operating at higher powers without suffering the same drop in performance as seen in metal based grids.

Figure 7 provides a direct comparison of the equilibrium fusion rates for the various cathode materials as a function of operating pressure. It is important to note the large disparity between the samples, with almost two orders of magnitude variation between stainless steel and graphite. The exact mechanism by which one material produces a larger fusion rate than another is not yet fully understood and is the topic of ongoing, unpublished work.[35]

The observed fusion rates were found to be largely insensitive to changes in pressure, and we attribute this insensitivity to the order in which experiments were conducted. Measurements began at higher pressure and were reduced over time, revealing the same hysteresis effects as found in Sec. III. Measurements were conducted over <30 min, far less than the characteristic desorption times measured previously.

V. CONCLUSIONS

The contribution of gaseous, surface, and embedded fusion to the observed fusion rate in deuterium fuelled IEC devices was studied. In the 1×10^{-4}–1×10^{-3} Torr low voltage (<40 kV) regime, the surface fusion was found to contribute up to almost 80% of the total fusion, dispelling the notion of central ion focus fusion.

The dependence on the cathode material was also examined with large discrepancies observed between the samples.

Graphite was found to give close to two orders of magnitude improvement in the observed fusion rate when compared to stainless steel, indicating the possibility for the construction of a new class of high performance IEC systems based on graphite.

[1]O. A. Lavrent'ev, "Lavrent'ev's proposal forwarded to the CPSU Central Committee on July 29, 1950," Phys.-Usp. **44**, 862 (2001).
[2]O. A. Lavrent'ev, Ukr. Fiz. Zh. **8**, 440 (1963).
[3]O. A. Lavrent'ev, Ann. N. Y. Acad. Sci. **251**, 152–178 (1975).
[4]P. T. Farnsworth, U.S. patent 2358402 (1966).
[5]P. T. Farnsworth, U.S. patent 3386883 (1968).
[6]R. L. Hirsch, J. Appl. Phys. **38**, 4522 (1967).
[7]R. L. Hirsch, Phys. Fluids **11**, 2486 (1968).
[8]R. L. Hirsch and G. A. Meeks, U.S. patent 3530497 (1970).
[9]J. Kipritidis and J. Khachan, Phys. Rev. E **79**, 026403 (2009).
[10]V. Damideh, A. Sadighzadeh, A. Koohi, A. Aslezaeem, A. Heidarnia, N. Abdollahi, F. Abbasi Davani, and R. Damideh, J. Fusion Energy **31**, 109–111 (2012).
[11]G. H. Miley, J. Javedani, Y. Yamamoto, R. Nebel, J. Nadler, Y. Gu, A. Satsangi, and P. Heck, AIP Conf. Proc. **299**(1), 675–689 (1994).
[12]E. Haji Ebrahimi, R. Amrollahi, A. Sadighzadeh, M. Torabi, M. Sedaghat, R. Sabri, B. Pourshahab, and V. Damideh, J. Fusion Energy **32**, 62–65 (2013).
[13]D. C. Donovan, D. R. Boris, G. L. Kulcinski, J. F. Santarius, and G. R. Piefer, Rev. Sci. Instrum. **84**(3), 033501 (2013).
[14]S. K. Murali, G. A. Emmert, J. F. Santarius, and G. L. Kulcinski, Phys. Plasmas **17**(10), 102701 (2010).
[15]J. H. Nadler, Y. B. Gu, and G. H. Miley, Rev. Sci. Instrum. **63**(10), 4810–4812 (1992).
[16]A. S. Bölükdemir, Y. Akgün, and A. Alaçakir, J. Fusion Energy **32**(5), 561–565 (2013).
[17]T. Takamatsu, K. Masuda, T. Kyunai, H. Toku, and K. Yoshikawa, Nucl. Fusion **46**(1), 142 (2006).
[18]J. Khachan and S. Collis, Phys. Plasmas **8**(4), 1299–1304 (2001).
[19]J. Khachan, D. Moore, and S. Bosi, Phys. Plasmas **10**, 596 (2003).
[20]O. Shrier, J. Khachan, S. Bosi, M. Fitzgerald, and N. Evans, Phys. Plasmas **13**, 012703 (2006).
[21]J. Kipritidis, J. Khachan, M. Fitzgerald, and O. Shrier, Phys. Rev. E **77**, 066405 (2008).
[22]K. Christmann, O. Schober, G. Ertl, and M. Neumann, J. Chem. Phys. **60**(11), 4528–4540 (1974).
[23]P. W. Tamm and L. D. Schmidt, J. Chem. Phys. **55**(9), 4253–4259 (1971).
[24]S. M. Ko and L. D. Schmidt, Surf. Sci. **42**, 508–524 (1974).
[25]A. Y. Didyk, R. Wiśniewski, K. Kitowski, V. Kulikauskas, T. Wilczynska, A. Hofman, A. A. Shiryaev, and Y. V. Zubavichus, Phys. Part. Nucl. Lett. **9**(1), 86–95 (2012).
[26]B. B. Cipiti, "The fusion of advanced fuels to produce medical isotopes using electrostatic confinement," Doctoral thesis (University of Wisconsin, 2004).
[27]K. Masuda, T. Fujimoto, T. Nakagawa, H. Zen, T. Kajiwara, K. Nagasaki, and K. Yoshikawa, "Diagnostic system development for d-d and d-3he reaction distributions in an inertial-electrostatic confinement device by collimated proton measurements," Fusion Sci. Technol. **56**(1), 528–532 (2009).
[28]K. Noborio, S. Konishi, T. Maegawa, and Y. Yamamoto, "Numerical calculation of reactions on electrode surfaces and in a volume of a discharge type fusion neutron source," in *Proceedings of IEEE/NPSS 24th Symposium on Fusion Engineering* (June 2011), pp. 1–5.
[29]K. Noborio, Y. Yamamoto, and S. Konishi, Fusion Sci. Technol. **52**(4), 1105–1109 (2007).
[30]J.-P. Wulfkühler and M. Tajmar, "Novel inertial electrostatic confinement fusion with buckyball-shaped multi-grids," AIAA Paper 2016-4777, 2016.
[31]V. Mares and H. Schraube, Nucl. Instrum. Methods Phys. Res., Sect. A **337**(2), 461–473 (1994).
[32]K. Nobe, H. Imaji, K. Nanjo, W. Ngamdee, M. Watanabe, and E. Hotta, in Proceedings of 14th US-Japan Workshop on IECF (2012).
[33]E. Tal-Gutelmacher, D. Eliezer, and E. Abramov, Mater. Sci. Eng., A **445–446**, 625–631 (2007).
[34]L. B. Begrambekov, A. A. Ayrapetov, Y. A. Sadovskiy, and P. A. Shigin, J. Phys.: Conf. Ser. **669**(1), 012003 (2016).
[35]J. Builth-Williams, "Geometrically and reflectively enhanced embedded fusion," Doctoral thesis (University of Sydney, 2018) (unpublished).